Diyala Journal of Engineering Sciences

Journal homepage: https://djes.info/index.php/djes

ISSN: 1999-8716 (Print); 2616-6909 (Online)

Design and Performance Optimization of a 3D-Printed SIW Antenna for Free-Space Applications

Md Mahabub Alam[1], Nurhafizah Abu Talip Yusof[1,3*], Nurazyyati Inas[2], Muhammad Naim Aminuddin[1], Bifta Sama Bari[1], Yasmin Abdul Wahab[1], Mohamad Shaiful Abdul Karim[1]

[1] Faculty of Electronic Engineering Technology, Universiti Malaysia Pahang Al-Sultan Abdullah, 26600 Pekan, Pahang, Malaysia
[2] Brownfield Engineering Sdn. Bhd., No.21, Jalan Teknologi 3/3A Taman Sains Selangor 1, Pju 5 Kota Damansara, 47810 Petaling Jaya, Selangor
[3] Center for Research in Advanced Fluid & Processes (Fluid Center), Universiti Malaysia Pahang Al-Sultan Abdullah, Lebuh Persiaran Tun Khalil Yaakob, 26300 Kuantan, Pahang, Malaysia

ARTICLE INFO

Article history:
Received October 12, 2024
Revised February 23, 2025
Accepted February 28, 2025
Available online March 1, 2025

Keywords:
Antenna
SIW
Free-space concept
PLA
Scattering parameter

ABSTRACT

This paper presents the design and performance evaluation of a Substrate-Integrated Waveguide (SIW) antenna fabricated using 3D printing technology, with a focus on optimizing its performance for future free-space applications. The proposed antenna integrates an SIW structure with a horn antenna concept, effectively combining the transmitter and receiver functions into a compact, monolithic substrate. This approach provides a miniaturized alternative to conventional free-space material characterization setups, leveraging SIW technology to replace bulky horn antennas with integrated structures. The study demonstrates the feasibility of compact free-space techniques for non-destructive testing, sensing, and electromagnetic material characterization applications. The study involves modeling and simulation using Computer Simulation Technology (CST) software, focusing on antenna performance in the G-band range (4–6 GHz). The fabricated prototype demonstrates resonant frequencies at 5.02 GHz and 6.0 GHz, with a scattering parameter below -10 dB and a well-defined radiation pattern, exhibiting sidelobes at -2.7 dB. The antenna is fabricated using biodegradable Polylactic Acid (PLA) material, reinforcing the potential for sustainable electronics while maintaining structural integrity and electromagnetic compatibility. While this study does not yet validate the antenna for material characterization, the results confirm its feasibility as a compact, cost-effective alternative to conventional free-space setups. This work lays the foundation for further optimization and experimental validation, advancing the role of 3D-printed SIW antennas in free-space applications.

1. Introduction

Substrate-Integrated Waveguide (SIW) antennas fabricated using 3D printing technology represent a significant advancement in electromagnetic design and manufacturing [1-2]. These antennas offer several advantages, including compact size, cost-effectiveness, and excellent performance for high-frequency applications, making them suitable for modern communication and sensing technologies [3-5]. SIW technology combines the benefits of microstrip and waveguide structures, providing reduced radiation losses, improved stability, and efficient power handling in electromagnetic wave transmission applications.

One emerging application of SIW antennas is in free-space measurement techniques, which conventionally rely on separate, bulky horn antennas for material characterization and

* Corresponding author.
E-mail address: hafizahs@umpsa.edu.my
DOI: 10.24237/djes.2025.18110

This work is licensed under a Creative Commons Attribution 4.0 International License.

electromagnetic property analysis [6-8]. Conventional free-space setups involve transmitter and receiver antennas positioned at a fixed distance to analyze the dielectric properties of a material placed in between. While effective, these systems are often large, expensive, and require precise alignment, limiting their practical integration into compact sensing platforms [9-11]. A more integrated approach using SIW antennas could provide a miniaturized and cost-efficient alternative to conventional free-space setups, improving system flexibility while maintaining high-frequency performance.

Recent advancements in 3D printing technology have enabled the fabrication of SIW antennas with complex geometries, offering new possibilities for antenna miniaturization and sustainability [12-15]. However, optimizing the design and performance of 3D-printed SIW antennas remains a critical challenge, particularly in ensuring reliable electromagnetic characteristics while minimizing fabrication constraints [16-19].

This paper presents a preliminary study on the design and performance evaluation of a 3D-printed SIW antenna, focusing on its potential as a compact alternative for free-space applications. The antenna integrates an SIW structure with a horn antenna concept, aiming to enhance gain and directivity within a single substrate. The study involves modeling and simulation using Computer Simulation Technology (CST) software, evaluating its performance in the G-band range (4–6 GHz). The antenna achieves resonant frequencies at 5.02 GHz and 6.0 GHz, with a scattering parameter below -10 dB and a well-defined radiation pattern, exhibiting sidelobes measured at -2.7 dB. Fabrication is carried out using Polylactic Acid (PLA) to highlight sustainability aspects. While this work does not yet validate the antenna for material characterization, it demonstrates the feasibility of a more compact and integrated free-space measurement setup.

The rest of this paper is organized as follows: Section 2 reviews relevant literature on SIW antenna performance and their applications. Section 3 outlines the antenna design methodology, including integrating the SIW and horn antenna concepts and the fabrication procedure using 3D printing technology. Section 4 presents the results and analysis, while Section 5 compares the findings with previous works. Finally, Section 6 concludes the paper by summarizing significant insights and discussing potential future optimizations for SIW antennas in free-space applications.

2. Related work

Various antenna technologies have been explored to enhance performance parameters such as gain, bandwidth, and efficiency. Among them, SIW antennas have gained significant attention due to their compact structure, low-loss characteristics, and suitability for high-frequency applications. However, despite these advantages, SIW antennas often suffer from gain limitations and narrow bandwidth, necessitating further optimization.

Several studies have attempted to enhance SIW antenna performance using different design techniques. Amer et al. (2018) [20] developed a cavity-backed slot SIW antenna, achieving a gain of 6.35 dB. While this demonstrated improved performance, conventional antennas typically exhibit higher gains, highlighting the need for further modifications. Alnaiemy et al. (2020) [21] addressed this by incorporating electromagnetic bandgap (EBG) structures, enhancing the boresight gain from 1.5 dBi to 11.2 dBi at 5.8 GHz and increasing aperture efficiency from 4.1% to 38.8%. Similarly, Anusha et al. (2021) [22] integrated Split-Ring Resonators (SRR) into microstrip antennas, significantly improving both gain and bandwidth.

Beyond these techniques, recent advancements in SIW structures have explored novel approaches for performance improvement. Jin et al. (2024) [23] introduced a slow-wave SIW resonator, demonstrating enhanced efficiency and reduced losses compared to conventional planar transmission lines. Meanwhile, Chen et al. (2023) [24] investigated flexible SIW resonators incorporating nanodiamond materials, achieving higher gain and lower hysteresis,

though flexibility introduced additional fabrication challenges. Additionally, Amiri et al. (2021) [25] explored metamaterial-based SIW antennas to improve radiation characteristics, demonstrating high precision in wave propagation control, though bandwidth constraints and environmental interference remained significant hurdles.

Table 1: Summary of SIW-based antenna studies and their performance enhancements

Ref.	SIW Type	Performance Highlights	Application
[20]	Cavity-backed slot SIW	Gain: 6.35 dB	Antenna performance optimization
[21]	SIW with EBG structure	Gain: 1.5 → 11.2 dBi; Efficiency: 4.1% → 38.8%	Bandwidth & gain enhancement
[22]	SIW with SRR integration	Significant gain and bandwidth improvement	High-efficiency antenna design
[23]	Slow-wave SIW resonator	Enhanced efficiency, reduced loss.	Antenna miniaturization.
[24]	Flexible SIW with nanodiamonds	High gain, low hysteresis.	Flexible antenna applications
[25]	Metamaterial-based SIW	High precision wave propagation	Electromagnetic performance improvement

These studies, summarized in Table 1, underscore the ongoing efforts to optimize SIW antenna performance, particularly in terms of gain enhancement, bandwidth expansion, and structural integration. However, further innovation is required to improve efficiency for free-space applications, where minimizing losses and maximizing radiation effectiveness are crucial. The next section discusses the proposed design, which leverages 3D printing technology to achieve enhanced performance, sustainability, and structural flexibility.

3. Methodology

The proposed 3D-printed SIW antenna is designed based on fundamental SIW antenna principles and optimized using CST software. This section outlines the systematic approach to antenna design, simulation, optimization, and fabrication, ensuring its suitability for free-space applications and material characterization.

The methodology begins with modeling an SIW-based horn antenna, followed by performance optimization. Initially, the design was simulated using FR-4 as the substrate material. However, for alignment with fabrication feasibility and sustainability, PLA was selected for both simulation and fabrication. The PLA substrate integrates two horn antennas, with their spacing adjusted to optimize electromagnetic wave propagation and minimize signal loss. The antenna's performance was evaluated under different configurations to refine its response, particularly by analyzing the spacing between the horns and its impact on transmission characteristics. Performance metrics, including scattering parameters (S-parameters), were assessed to ensure efficient operation, targeting S_{11} values below -10 dB for minimal signal loss [26]. Once the design was optimized, the antenna was fabricated using PLA and tested experimentally. The measured results were compared with simulations to validate the design and assess its potential for future sensing applications, particularly in free-space characterization setups.

3.1 Theoretical Basis for SIW Design

The SIW operates similarly to a conventional rectangular waveguide but offers the advantage of being integrated onto a planar dielectric substrate. A waveguide is a physical structure that confines and directs electromagnetic waves, with specific propagation characteristics, defined by its boundaries [27-28]. In a waveguide, the mode of propagation depends on the structure's geometry and the frequency of the wave. The two primary waveguide modes are Transverse

Electric (TE) and Transverse Magnetic (TM). In TE mode, the electric field is entirely transverse to the direction of propagation, meaning there is no electric field component in the propagation direction. In contrast, in TM mode, the magnetic field is entirely transverse, implying that the electric field has a component in the direction of wave propagation. In an SIW structure, rows of conducting vias are embedded in a dielectric substrate between two metallic plates, forming a guiding structure that confines electromagnetic waves within the substrate. This configuration ensures effective signal transmission while maintaining a compact and planar form factor, making it highly suitable for integration into modern electronic systems. The design of an SIW antenna follows classical waveguide theory, where the cutoff frequency plays a fundamental role in defining its operational characteristics. The cutoff frequency, denoted as f_c, represents the lowest frequency at which the waveguide allows propagation. The cutoff frequency for a rectangular waveguide is given by Eq. (1). Figure 1 depicts the basic structure of the SIW antenna.

$$f_c = \frac{c}{2\pi}\sqrt{\left(\frac{m\pi}{W_{eq}}\right)^2 + \left(\frac{n\pi}{L_{eq}}\right)^2} \quad (1)$$

Where c is the speed of light, m and n are the mode indices, and W_{eq} and L_{eq} are the equivalent width and length of the SIW. This equation defines the frequency at which the waveguide transitions from cutoff to propagation.

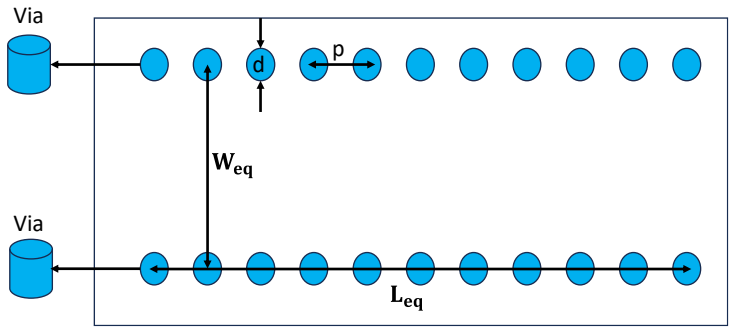

Figure 1. Basic structure of SIW antenna design [29].

In the design process, the width of the waveguide, W_{eq}, is an important parameter, and it is determined by Eq. (2) [29].

$$W_{eq} = w - \frac{d^2}{0.95p} \quad (2)$$

where w is the waveguide width, d is the diameter of the vias, and p is the distance between the vias. These parameters must be carefully optimized to ensure the desired performance of the antenna. A key design constraint for SIW structures is the ratio of the via diameter (d) to the waveguide width (w). To maintain effective waveguide operation, this ratio is typically kept below 2, as defined by Eq. (3) [3].

$$\frac{d}{w} < 2 \quad (3)$$

If the ratio of $\frac{d}{w}$ becomes too large, it can significantly reduce the effective width of the waveguide, thereby limiting the ability to confine the electromagnetic waves and affecting the overall antenna performance.

Similarly, the distance between the vias, represented by p, is another important parameter. The ratio of via pitch (p) to via diameter (d) is crucial for ensuring proper wave confinement. To avoid leakage, this ratio should not exceed 2.5, as expressed by Eq. (4). If the ratio $\frac{p}{d}$ exceeds 2.5, the gaps between the vias may allow significant electromagnetic wave leakage, which can degrade the waveguide's performance and reduce energy confinement[3].

$$\frac{p}{d} < 2.5 \quad (4)$$

To reduce return and leakage losses, it was determined that the diameter of the hole needed to fulfil certain geometric limitations, defined by Eqs. (5) and (6) [29].

$$d < \frac{\lambda_g}{5} \quad (5)$$

$$p \leq 2d \quad (6)$$

Here, λ_g is the guided wavelength, which represents the wavelength of the signal within the waveguide. It is shorter than the free-space wavelength λ_0 due to the dielectric material of the substrate. The condition $d < \frac{\lambda_g}{5}$ ensures that the via diameter is sufficiently small to maintain proper wave confinement, minimize leakage, and preserve the SIW's desired performance characteristics. The condition $p<2d$ also defines the relationship between the via pitch (p) and the via diameter (d), where p is the distance between the centres of adjacent vias, and d is the diameter of each via. This ensures the vias are sufficiently close to minimize leakage and maintain effective waveguiding behavior.

In this study, the SIW antenna design adheres to these theoretical principles to optimize wave confinement and signal propagation. By carefully selecting and adjusting significant parameters such as via size, spacing, and equivalent width, the proposed design aims to achieve efficient electromagnetic performance with minimal signal loss, ensuring reliable operation in future sensing applications.

3.2 Simulation of the proposed antenna design configuration and their analysis

The proposed SIW antenna design incorporates principles derived from the free-space method, which have been adapted into a configuration featuring horn antennas integrated onto a single substrate. To evaluate the antenna's performance and refine its structural parameters, simulations were conducted using CST software. These simulations examined various configurations to optimize wave propagation efficiency and minimize signal loss. Initially, the antenna was designed using an FR-4 substrate, consistent with standard waveguide fabrication methods. However, to align the simulation results with the material intended for fabrication, the FR-4 substrate was replaced with PLA. The decision to use PLA was influenced by its compatibility with sustainable 3D printing techniques, which provide both precision and environmental benefits.

3.2.1 Basic Design of the Proposed SIW Antenna

The development of the proposed SIW antenna began with a validation phase to ensure that the simulation methodology accurately captured the intended electromagnetic behavior. The initial design followed the structure of a reference SIW antenna, which served as a fundamental framework for comparison and improvement.

In the first phase of simulation, FR-4 was used as the substrate material, replicating the basic SIW design to confirm the effectiveness of CST software for modeling the structure. The basic SIW antenna, as illustrated in Figure 2(a), consists of a dielectric substrate with two rows of conducting vias forming the waveguide. This configuration acts as a guided transmission line for electromagnetic waves, making it a straightforward and efficient design for initial validation. To enhance performance, the SIW structure was modified by integrating a horn-shaped extension at both ends, as shown in Figure 2(b). This modification aimed to improve the resonant frequency response and overall efficiency of the antenna. The horn sections serve as transmitter and receiver components, inspired by the free-space method's approach to electromagnetic wave propagation. The transition from a standard SIW structure to a horn-shaped SIW antenna allows for better impedance matching and higher gain, resulting in improved radiation characteristics. The dimensions of the basic SIW horn antenna are summarized in Table 2. The structure includes circular vias with a diameter (d) of 1.00 mm, spaced at a pitch (p) of 4.70 mm between consecutive vias in the same row. The vertical spacing (a) between the rows of vias is 12.76 mm. The overall width (W) is 160.00 mm, while the total length (L_T) is 170.00 mm, divided into two sections: a feed length (L_1) of 42.05 mm and a flare length (L_2) of 121.49 mm.

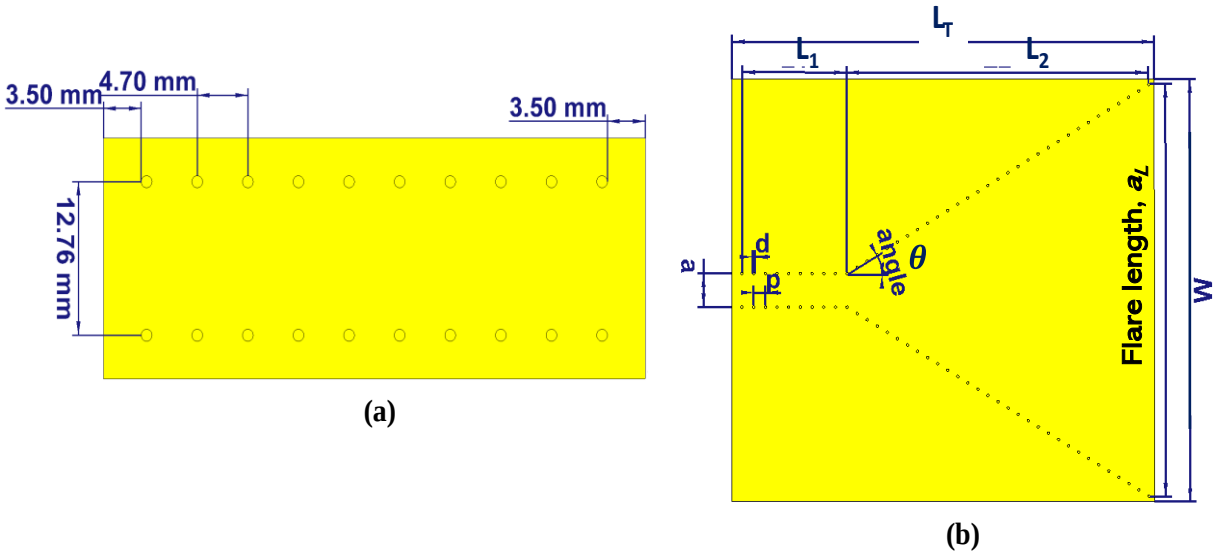

Figure 2. Proposed SIW Design in CST (a) Basic SIW Antenna (b) SIW Horn Antenna.

Table 2: Parameters of Basic SIW Horn Antenna.

Parameters	Dimensions (mm)
Diameter of hole, ***d***	1.00
Distance between 2 via (pitch), ***p***	4.70
Distance between 2 rows of via, ***a***	12.76
Total width, **W**	160.00
Length of feed, $\mathbf{L_1}$	42.05
Length of flare, $\mathbf{L_2}$	121.49
Total length, $\mathbf{L_T}$	170.00
Flare length, $\boldsymbol{a_L}$	156.39
Substrate thickness, $\mathbf{z_s}$	1.62
Flare angle, $\boldsymbol{\theta}$	30.50°

The flare section, designed with a flare angle (θ) of 30.50°, results in a calculated flare length (a_L) of 156.39 mm. The substrate thickness (Z_s) is 1.62 mm.

By comparing the performance of the basic SIW structure with the modified horn-shaped design, the simulations confirmed that the horn-shaped antenna offered a significant improvement in resonant frequency response and impedance matching. These findings validated the simulation approach and established a strong foundation for further enhancements, which are explored in the next phase of design modifications.

3.2.2 Implementation of the Free-space Method in the Proposed SIW Antenna Design

Building on the validated horn-shaped SIW antenna design, the next phase of the study involved integrating the transmitter and receiver onto a single substrate, inspired by the free-space measurement method [30-32]. This stage aimed to optimize the antenna's configuration before transitioning from FR-4 to PLA for fabrication. The proposed setup consists of two identical horn antennas positioned symmetrically on the same substrate, ensuring balanced performance and efficient wave transmission.

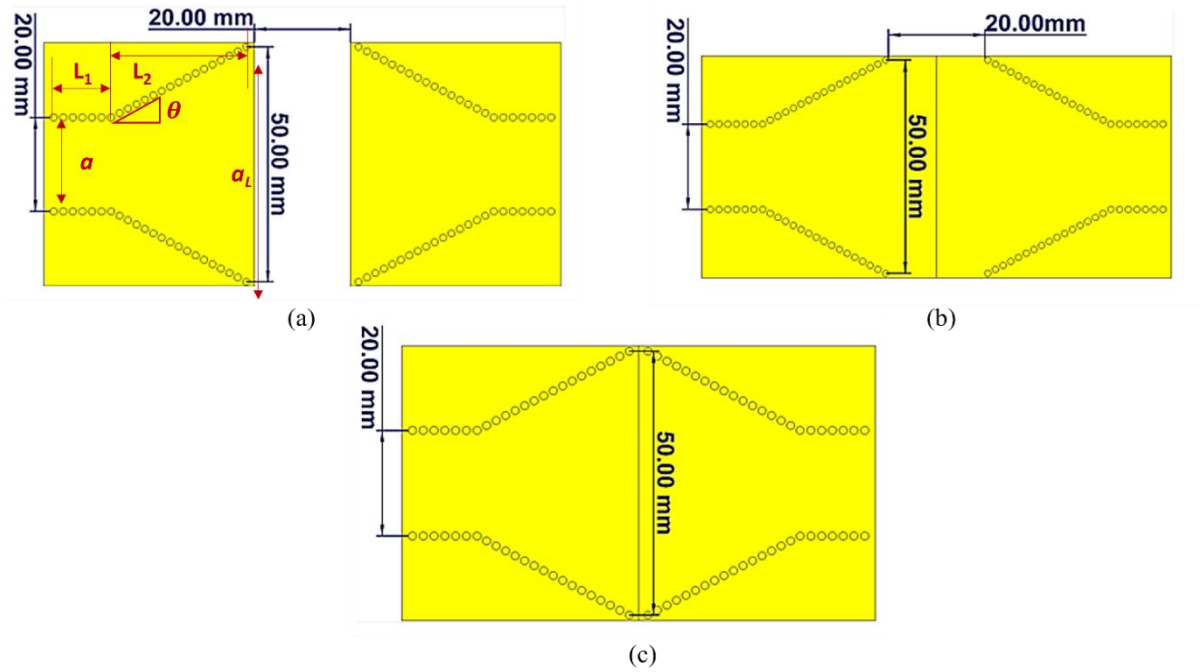

Figure 3. Proposed SIW two-horn antenna with varied configuration (a) 20mm gap; (b) 20mm loading; and (c) no loading.

.

This configuration was designed to evaluate the antenna's response under different arrangements and to determine the most effective way to facilitate free-space wave propagation. Three different configurations were implemented and analyzed through simulation to assess the effectiveness of the free-space method, as illustrated in Figure 3. The first configuration (Figure 3a) introduced a 20-mm gap between the two horn antennas to simulate a scenario where spatial separation influences electromagnetic wave transmission. The second configuration (Figure 3b) incorporated a 20-mm loading section between the two horns, enhancing electromagnetic coupling and interaction. The third configuration (Figure 3c) completely eliminated the gap, forming a continuous structure that maximized integration and minimized signal loss.

To achieve optimal performance, the parameters of the horn antennas were systematically adjusted, with their detailed dimensions provided in Table 3. Each horn structure consists of circular vias with a diameter (d) of 1.50 mm, evenly spaced at a pitch (p) of 2.00 mm. The vertical spacing (a) between the rows of vias measures 20.00 mm. The total length of the antenna is divided into two sections: a feed section (L_1) measuring 11.65 mm and a flared horn section (L_2) measuring 28.27 mm. The flare section is designed with a flare angle (θ) of 27.95°, leading to a calculated flare length (a_L) of 50.00 mm.

By analyzing the results obtained from these three configurations, the study focused on understanding how integrating the two horn antennas onto a single substrate affected overall antenna performance. The simulations provided valuable insights into the ability of each configuration to maintain efficient wave propagation while minimizing unwanted reflections and losses. These findings served as a foundation for finalizing the design and transitioning to PLA as the dielectric material in the subsequent phase.

Table 3: Dimensions for parameters of single SIW horn antenna

Parameters	Dimensions (mm)
Diameter of hole, d	1.50
Distance between 2 via (pitch), p	2.00
Distance between 2 rows of via, a	20.00
Length of feed, L_1	11.65
Length of flare, L_2	28.27
Flare length, a_L	50
Substrate thickness, Z_s	1.60
Flare angle, θ	27.95°

3.2.3 Final Proposed SIW Antenna Design

After evaluating the performance of the horn antenna configurations, particularly those shown in Figures 3b and 3c, the study focused on further refining the SIW antenna design to enhance its structural integration and ensure suitability for free-space applications. One of the critical considerations in this refinement was the selection of a suitable substrate material, as it directly influences the antenna's electromagnetic performance, fabrication feasibility, and environmental impact. While conventional antenna substrates, such as FR-4 and Rogers laminates, are widely used due to their stable dielectric properties, they also come with certain limitations. FR-4, for example, is cost-effective but exhibits higher dielectric losses, whereas Rogers materials provide superior electrical performance but at a significantly higher cost.

In this study, Polylactic Acid (PLA) was selected as the dielectric material due to its balance between performance, fabrication flexibility, and sustainability. Compared to traditional substrates, PLA offers unique advantages that make it a viable alternative for 3D-printed antenna applications. In terms of dielectric properties, PLA exhibits a loss tangent ($\tan\delta = 0.001$), which is lower than that of FR-4 ($\tan\delta = 0.02$), leading to reduced dielectric losses, improved radiation efficiency, and minimal signal attenuation [33]. Although Rogers laminates have an even lower loss tangent ($\tan\delta < 0.002$), their high cost and specialized manufacturing requirements make them less practical for rapid prototyping and cost-sensitive applications. Furthermore, PLA's relative permittivity ($\varepsilon_r = 3.549$) is lower than that of FR-4 ($\varepsilon_r = 4.4$), which helps to minimize impedance mismatches and improve bandwidth, while also contributing to better gain performance compared to FR-4-based designs [34].

Beyond its electrical properties, PLA's compatibility with 3D printing makes it particularly advantageous for fabricating intricate antenna structures that would be challenging to achieve using conventional PCB-based FR-4 or Rogers substrates [35]. The ability to manufacture antennas with high precision and complex geometries directly impacts performance optimization, especially for applications requiring customized waveguiding structures. However, despite these benefits, PLA does have lower temperature stability compared to Rogers laminates, which could affect long-term performance under extreme environmental conditions. Nevertheless, for the intended application, PLA offers sufficient mechanical rigidity and dimensional stability to ensure practical usability. In addition to its electrical and fabrication advantages, PLA stands out as an environmentally sustainable alternative. Unlike FR-4 and Rogers laminates, which contribute significantly to electronic waste, PLA is biodegradable and recyclable, making it an attractive option for sustainable engineering applications. Furthermore, it provides a cost-

effective alternative, offering better performance than FR-4 while remaining significantly more affordable than Rogers materials. This combination of dielectric performance, fabrication feasibility, and environmental benefits positions PLA as a promising substrate for next-generation antenna technologies, particularly those leveraging additive manufacturing techniques.

To achieve optimal performance, the design parameters were fine-tuned based on insights gained from the previous configurations. The finalized antenna design, as detailed in Figure 4 and Table 4, features an overall width (W) of 74.00 mm and a total length (L_T) of 114.00 mm. This length is divided into two sections: a feed section (L_1) measuring 10.70 mm and a flared section (L_2) measuring 23.00 mm. The flare section has a flare angle (θ) of 17.00°, resulting in a calculated flare length (a_L) of 68.47 mm. Additionally, a loading section was introduced between the two horn shaped antennas, serving to enhance structural integrity and functional integration.

The final design reflects the most optimized configuration achieved in this study, ensuring effective signal transmission with minimal losses.

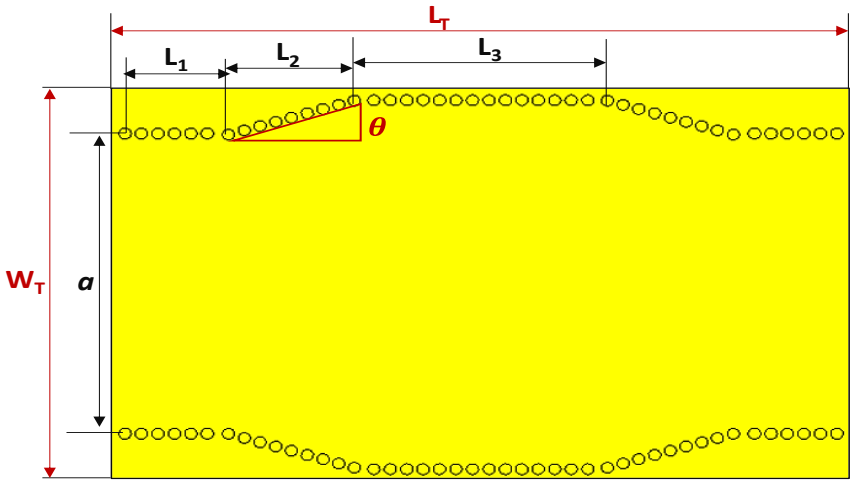

Figure 4. Final design of our proposed SIW horn antenna in CST.

Table 4: Dimensions for parameters of free-space concept SIW antenna

Parameters	Dimensions (mm)
Diameter of hole, d	2.00
Distance between 2 via (pitch), p	2.67
Distance between 2 rows of via, a	55.00
Total width, W	74.00
Length of feed, L_1	10.70
Length of flare, L_2	23.00
Length of loading, L_3	42.00
Total length, L_T	114.00
Flare length, a_L	68.47
Flare angle, θ	17.00°

While this study primarily focuses on validating the antenna's design and performance, the structure also allows for future applications where a Material Under Test (MUT) could be placed between the two horns for sensing and measurement purposes. The simulation results confirm that the proposed antenna configuration meets the desired performance criteria, demonstrating its feasibility for free-space applications. With this optimized design finalized, the next stage involves fabricating the antenna and conducting experimental validation, which will be detailed in Section 3.3.

3.3 Fabrication of 3D-printed SIW Antenna

The final design of the SIW horn antenna was fabricated using an Ender 5 3D printer with PLA filament. PLA was selected due to its compatibility with 3D printing, eco-friendly nature, and recyclability, aligning with sustainable fabrication practices [36-37]. The antenna components were first designed and simulated in CST software before being exported in STL format. These files were then imported into Ultimaker Cura software for slicing and configuring the 3D printer settings. To ensure precision and structural integrity, the fabrication process utilized a 0.4 mm nozzle, with a layer height of 0.2 mm, a printing temperature of 200°C, a build plate temperature of 90°C, and an infill density of 90%. The fabrication sequence is illustrated in Figure 5, detailing each stage of the antenna assembly. The process began with the printing of the base substrate (Figure 5a), which formed the foundation of the SIW antenna structure. Once the substrate was fabricated, copper tape was applied to its surface to establish the conductive layer necessary for SIW wave propagation (Figure 5b). Copper tape was chosen due to its excellent electrical conductivity and ease of application, ensuring a uniform conductive surface. For the implementation of the SIW vias, copper rivets were used to create electrical connections between the top and bottom conductive layers. Approximately 80 copper rivets were manually inserted into the pre-printed via holes on the substrate (Figure 5c). This step was crucial for maintaining the integrity of the SIW structure, as the rivets provided both mechanical stability and electrical continuity across the layers.

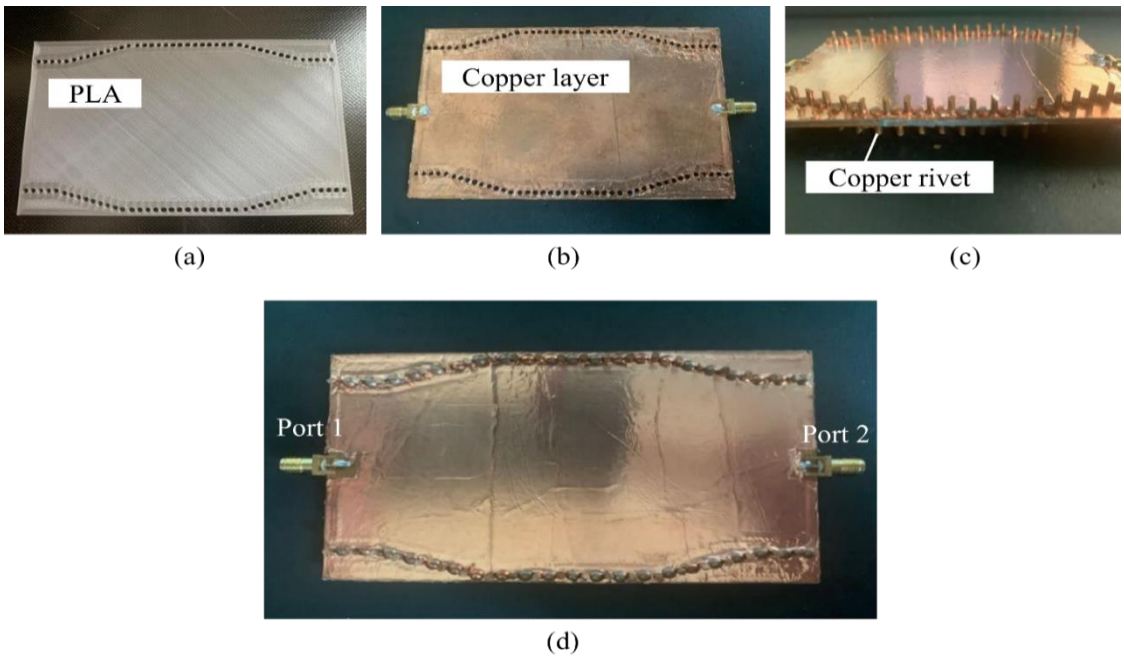

Figure 5. Fabricated view (physical) of our proposed SIW antenna (a) base substrate (b) wrapped substrate with copper tape (c) copper rivet placed at via hole (d) final prototype of SIW antenna.

Finally, the two horn-shaped antennas were assembled and integrated onto the substrate, with two ports added to enable antenna operation (Figure 5d). The completed SIW horn antenna closely adhered to the CST simulation specifications, ensuring consistency between the designed and fabricated structures.

This fabrication approach demonstrates the feasibility of combining 3D printing with conventional conductive elements to develop SIW antennas. By utilizing PLA as the dielectric substrate, the process highlights an environmentally sustainable and cost-effective method for manufacturing advanced antenna structures, supporting the adoption of 3D-printed SIW antennas for future sensing applications.

4. Results and discussion

Scattering parameters (S-parameters) are fundamental in Radio Frequency (RF) and microwave engineering for analyzing signal behavior in multi-port networks. They describe the relationship between incident (input) and reflected (output) signals, forming a complex matrix that quantifies power transfer between ports. The S_{11} parameter represents the input reflection coefficient, indicating the amount of signal reflected at port 1, while S_{22} measures the reflection at port 2. The S_{21} parameter defines the forward transmission coefficient, representing the fraction of the signal propagating from port 1 to port 2, whereas S_{12} describes the reverse transmission coefficient, indicating the signal propagation from port 2 back to port 1.

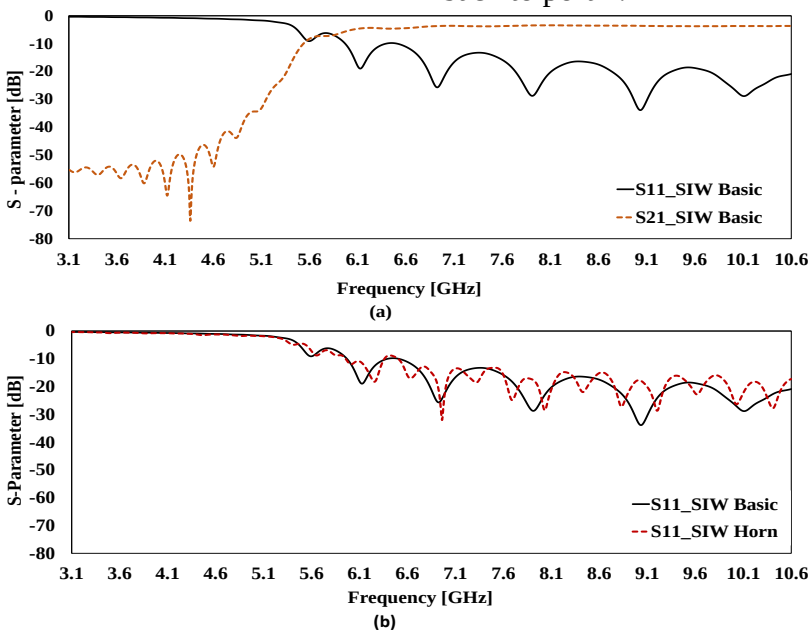

Figure 6. (a) S_{11} and S_{21} of SIW basic structure proposed work in CST (b) S_{11} comparison of SIW basic and horn structure proposed work in CST.

The proposed SIW antenna was designed and simulated using CST software with a targeted resonant frequency of 5.02 GHz. The reflection coefficient (S_{11}) and transmission coefficient (S_{21}) were analyzed to evaluate the antenna's performance. The horn antenna dimensions were optimized through detailed simulations, considering key parameters such as antenna length, width, and hole diameter. Initially, simulations were conducted using FR-4 as the dielectric material, but the design was later adapted for PLA fabrication. After completing the simulations, the antenna prototype was fabricated, and its performance was experimentally validated by comparing simulated and measured results.

4.1 Simulation Results

This section presents the simulation results for the proposed SIW antenna, focusing on the S_{11} and S_{21} parameters across different antenna configurations. Various design parameters were evaluated to determine the optimal configuration for enhanced performance.

4.1.1 Performance Analysis of the Basic SIW Antenna Design

The initial simulation of the basic SIW antenna was conducted to establish a reference for subsequent modifications. This involved analyzing the S_{11} and S_{21} parameters, which are crucial for assessing the antenna's transmission efficiency and reflection behavior. Figure 6(a) presents the simulated S_{11} and S_{21} results for the basic SIW structure. The S_{11} parameter remains below -10 dB across the 5.6 GHz to 10.6 GHz frequency range, with a dominant resonance observed at 9.1 GHz. This indicates efficient impedance matching over a broad bandwidth, ensuring stable operation within this range. In contrast, the S_{21} parameter exhibits high attenuation (-50 to -70 dB) below 5 GHz, transitioning to significantly lower attenuation above 5.6 GHz. This behavior confirms that the basic SIW structure functions as a bandpass filter, where signals below 5 GHz are effectively suppressed, while those in the passband (above 5.6 GHz) experience minimal transmission loss.

Figure 6(b) provides a comparative analysis of S_{11} parameters between the basic SIW antenna and the SIW horn antenna across the 3.1 GHz to 10.6 GHz frequency range. The basic SIW antenna demonstrates effective impedance matching within the 5.6 GHz to 10 GHz range, maintaining consistent resonant frequencies. However, the SIW horn antenna exhibits enhanced performance due to its flared-section design, which improves impedance matching and increases radiation efficiency. This structural modification facilitates a smooth transition from the narrow waveguide to a wider aperture, optimizing wave propagation and minimizing reflections. Additionally, the horn structure enables waveguide-to-free-space mode transitions, resulting in distinct electromagnetic field perturbations and more pronounced resonance characteristics. These improvements confirm that the SIW horn antenna provides superior impedance matching and radiation performance, making it a highly suitable candidate for high-frequency applications.

4.1.2 Simulation Results of the Free-space Method Implementation in SIW Antenna Designs

The simulated S-parameters using the concept of free-space method setup demonstrate the optimization process of the proposed SIW antenna through various structural modifications to the basic design. The performance was evaluated for three different configurations: a 20-mm gap, 20-mm loading, and no-loading condition. The results reveal distinct performance characteristics for each case. The SIW antenna with a 20-mm gap, as shown in Figure 7(a), exhibits an S_{11} parameter with a deep notch below -10 dB at 3.8 GHz, indicating excellent impedance matching and minimal signal reflection. Additionally, the S_{21} parameter shows high attenuation, approximately -70 dB, at lower frequencies, with continued attenuation in the range of -35 to -40 dB beyond 3.8 GHz, effectively preventing unwanted signal transmission. These characteristics confirm that the antenna performs optimally at 3.8 GHz, with strong rejection of signals at both lower and higher frequencies. In contrast, the 20-mm loaded SIW antenna, as illustrated in Figure 7(b), demonstrates significantly enhanced performance. The S_{11} parameter exhibits multiple resonances at 3.8 GHz, 4.5 GHz, and 5.5 GHz, with return losses around -30 dB, ensuring excellent impedance matching. The reflection coefficient remains below -10 dB above 4 GHz, indicating stable impedance matching across a broader frequency range.

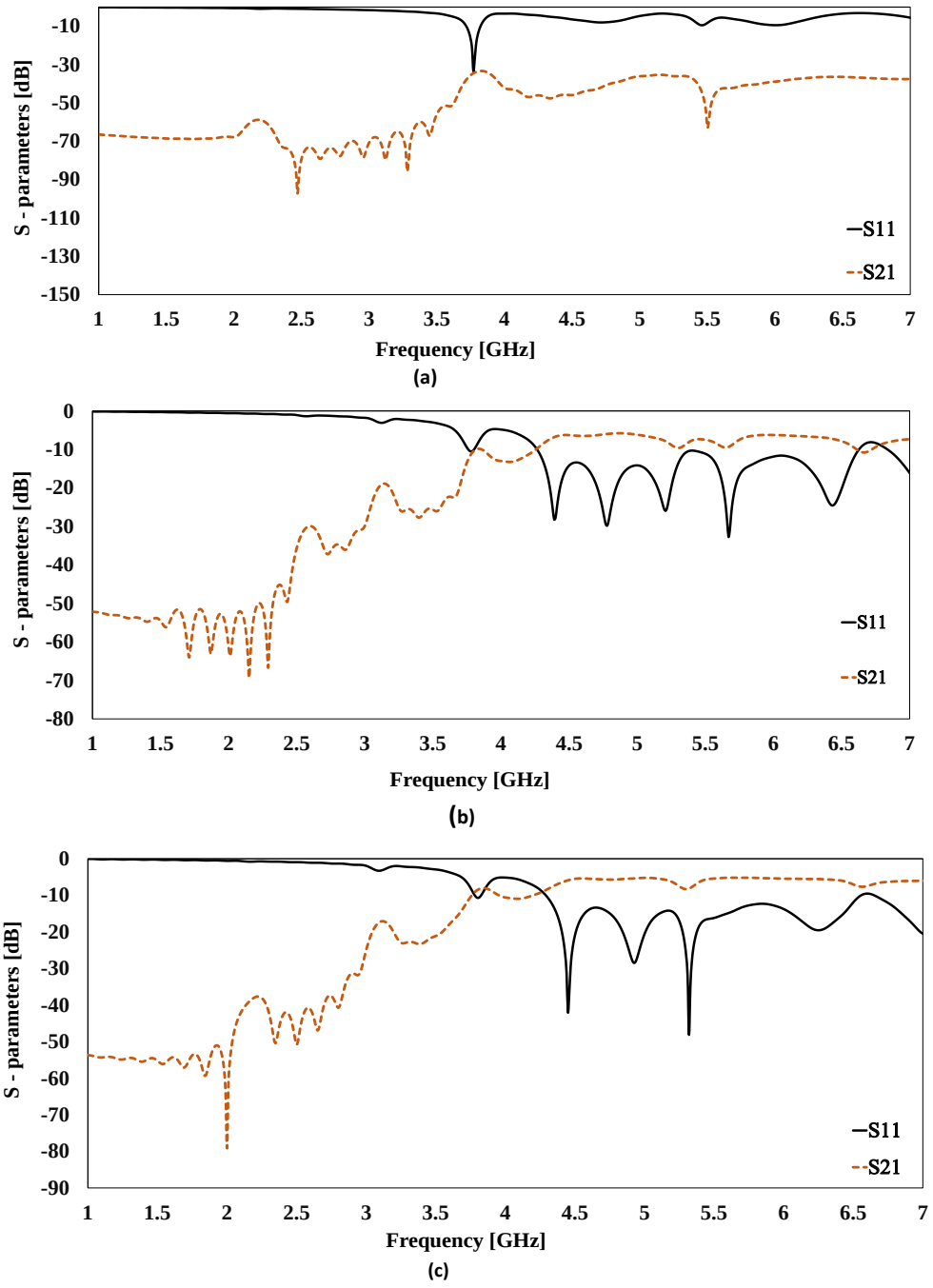

Figure 7. (a) S-parameter for configuration with a 20-mm gap. (b) S-parameter for configuration with 20 mm loading. (c) S-parameter for configuration with no loading.

The S_{21} parameter, on the other hand, shows strong isolation between 1.5 GHz and 2.5 GHz, followed by a gradual increase in transmission from 2.5 GHz to 4 GHz, and stable transmission in the range of -5 to -10 dB above 4 GHz, suggesting efficient power transfer. These results confirm that the 20-mm loading condition provides a high-pass filtering response while maintaining optimal impedance matching.

Meanwhile, the no-loading SIW antenna configuration, shown in Figure 7(c), also exhibits distinct performance characteristics. The S_{21} parameter maintains effective high-pass filtering similar to the loaded configuration, but the S_{11} parameter demonstrates even better impedance matching, with three distinct resonances occurring at 4.5 GHz, 5 GHz, and 5.5 GHz, reaching deeper notches of approximately -40 dB. The improved reflection

characteristics suggest that the unloaded SIW antenna achieves superior impedance matching and more pronounced resonances compared to the loaded design. A comparative analysis of all three configurations provides further insights into their overall performance. The 20-mm gap configuration, depicted in Figure 7(a), exhibits limited resonant behavior, achieving only two resonant frequencies at 3.77 GHz and 7.42 GHz, with respective return loss values of -33.4 dB and -40.4 dB. In contrast, the 20-mm loading configuration demonstrates a more advanced performance profile, featuring six resonant frequencies distributed between 4 GHz and 8 GHz, with a peak resonance magnitude of -32.7 dB at 5.67 GHz. This configuration exhibits broader resonance coverage in the 4–6 GHz range, enhanced ripple behavior, improved impedance matching, and superior frequency selectivity. The no-loading configuration, despite achieving significant resonances with peak return losses of -48 dB and -41.9 dB, falls short of the 20-mm loading configuration in terms of resonance consistency and the number of resonance points. Among all three configurations, the 20-mm loading condition emerges as the optimal choice due to its broader resonance range, superior impedance matching, and enhanced ripple characteristics within the 4–6 GHz frequency band. These findings provide valuable insights for further optimizing the final antenna design, which will be explored in detail in Section 4.1.3.

4.1.3 Simulation Results of Proposed Final SIW Antenna

The simulated results of the proposed final SIW antenna design, illustrated in Figure 8(a), demonstrate excellent scattering parameter performance across the 4–6 GHz frequency range. The antenna, designed with a single substrate and integrated transmitter-receiver configuration, achieves resonant frequencies at 5.02 GHz and 6 GHz, with return loss magnitudes of -52 dB and -44.3 dB, respectively. These values indicate strong impedance matching and minimal signal reflection, ensuring efficient energy transfer across the target frequency range. Moving to the antenna's radiation characteristics, Figures 8(b) and 8(c) present the radiation pattern and far-field directivity at 5 GHz. The 3D radiation pattern, as shown in Figure 8(b), highlights highly focused radiation in the desired direction, achieving a peak directivity of 5.43 dBi, demonstrating the antenna's effectiveness in high-frequency applications. Furthermore, the polar plot in Figure 8(c) reveals a well-defined main lobe cantered at θ = 23.0°, with a beamwidth of 30.1° and a low side lobe level of -2.7 dB, confirming stable directional performance. These results collectively validate the antenna's high directivity, narrow beamwidth, and low side lobe interference, making it suitable for targeted communication and directional signal applications.

4.1.4 Performance Analysis of SIW Horn Antenna Configurations

The evaluation of various SIW horn antenna configurations in the free-space method setup was conducted to analyze the impact of structural modifications on significant performance metrics, including resonance frequency, impedance matching, directivity, and bandwidth. The selection of appropriate design parameters played a crucial role in optimizing radiation characteristics and minimizing reflection losses.

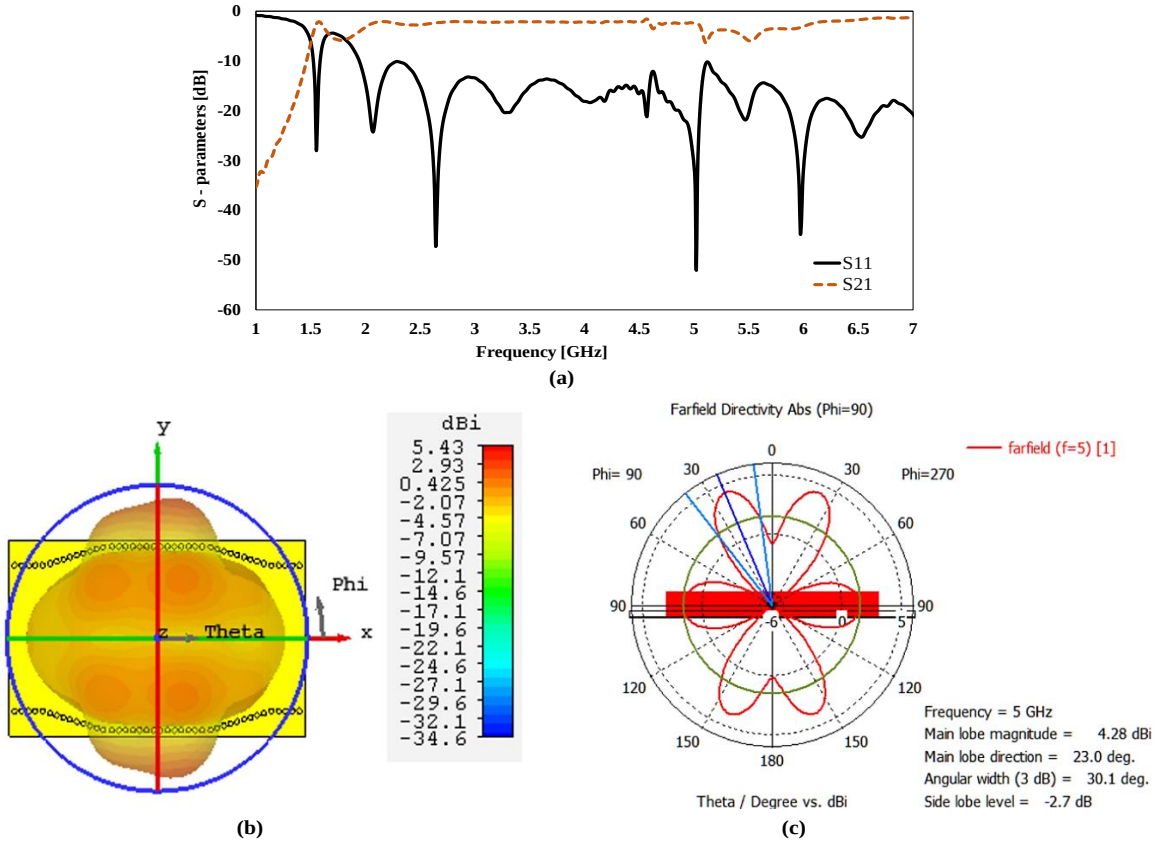

Figure 8. (a) S-parameter, (b) 3D radiation pattern, and (c) directivity at 5.02 GHz of final proposed SIW antenna.

Table 5: Comparison between different SIW horn antennas.

Antenna Configuration	Resonance Frequency (GHz)	Reflection Co-efficient (dB)	Maximum Directivity (dB)
Basic SIW horn	6.1,7.1,8.1,9.1	Below -15	5
SIW horn antenna with 20 mm load	3.8,4.5,5.5	-30	4.85
SIW horn antenna with no load	4.5,5,5.5	-40	5.18
Final SIW horn	5.02,6	-52 and -44	5.43

As shown in Table 5, the basic SIW horn antenna exhibited multiple resonances, with a reflection coefficient below -15 dB and a maximum directivity of 5 dBi. While this design provided a baseline for performance assessment, its impedance matching required further refinement. By incorporating a 20 mm loading section, the impedance matching improved significantly to -30 dB, enhancing overall efficiency. Additionally, an unloaded SIW horn antenna configuration demonstrated even better impedance characteristics, achieving a reflection coefficient of -40 dB and a directivity of 5.18 dBi.

The final optimized design, which integrated all significant refinements, exhibited superior performance, resonating at 5.02 GHz and 6 GHz with a reflection coefficient of -52 dB and -44 dB, respectively. This configuration also achieved the highest directivity of 5.43 dBi, demonstrating its suitability for free-space applications that require enhanced radiation efficiency and stable impedance matching. The integration of optimized structural elements allowed for improved wave propagation, reduced transmission losses, and enhanced radiation directivity, making it a highly efficient solution for compact, high-frequency applications.

To achieve the observed performance improvements, a systematic parametric tuning process was carried out using CST's built-in optimization tools. While heuristic optimization techniques such as Genetic Algorithms (GA), Particle Swarm Optimization (PSO), and Artificial Neural Networks (ANN) are commonly used for antenna design, this study specifically employed CST's parametric tuning due to its direct integration with electromagnetic simulation tools, enabling real-time adjustments to geometric parameters [38]. This approach ensures computational efficiency, as it allows rapid iteration without requiring extensive external computation and provides practical feasibility by allowing precise impedance matching within a single simulation environment. Given that the primary focus of this study was on structural modifications to improve antenna performance, heuristic-based approaches were beyond the intended scope. However, future research may explore such techniques to investigate multi-objective design optimizations, particularly in integrating additional variables such as advanced material properties and fabrication tolerances to further enhance antenna performance.

4.2.1 Results of Fabricated Antenna Measurement

After fabrication, the S_{11} and S_{21} parameters of the SIW antenna were measured using a VNA to assess its performance. Prior to measurement, the VNA was carefully calibrated with standard calibration tools to eliminate potential errors and ensure precise data acquisition. The two ports of the fabricated antenna were connected to the VNA through two-port connectors, and the scattering parameters were recorded. The measured S_{11} parameter, as illustrated in Figure 9, exhibits a significant drop below -10 dB within the 5 to 5.6 GHz frequency range, indicating effective impedance matching and minimal signal reflection within the desired operational band.

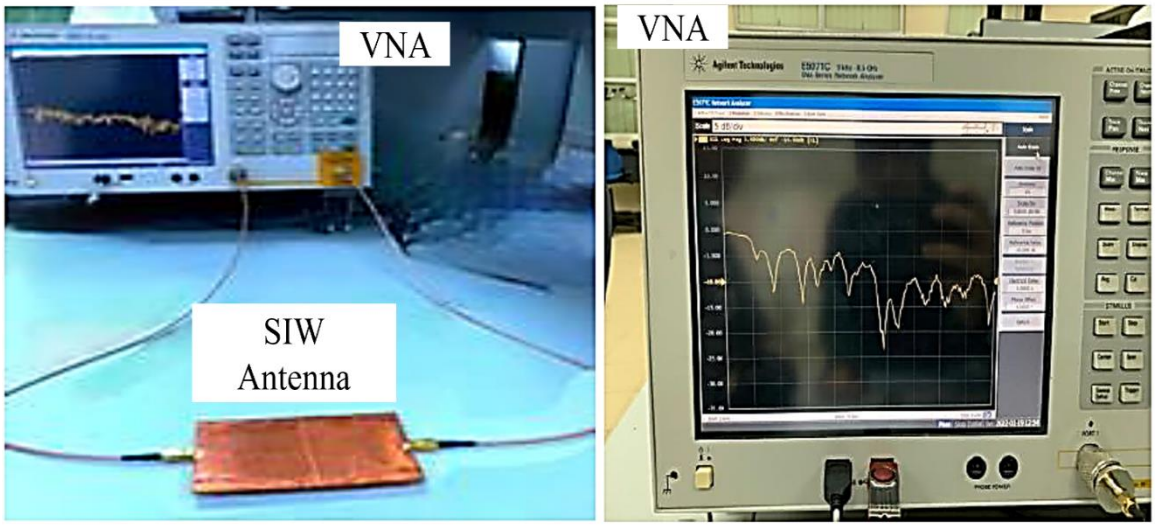

Figure 9. S-parameter (S_{11} and S_{21}) measurement setup for the final proposed fabricated antenna.

A comparative analysis between the measured and simulated S_{11} values reveals strong agreement, validating the design approach and confirming that the fabricated antenna closely follows the expected performance characteristics. The alignment between these results underscores the accuracy of the design methodology, demonstrating that the fabricated antenna effectively reflects the simulation outcomes into a functional prototype.

4.2.2 Validation of SIW Antenna Performance Based on the Simulation and Fabrication Results

To validate the fabricated antenna's performance, a direct comparison between the simulated and measured S_{11} and S_{21} parameters was conducted using data obtained from CST software and experimental measurements. This comparison ensures that the fabricated antenna

meets the intended design specifications while identifying any discrepancies between theoretical predictions and real-world implementation. As shown in Figures 10(a) and 10(b), the simulated and measured scattering parameters exhibit a strong level of agreement, confirming the antenna's expected performance. Examining the S_{11} parameter in Figure 10(a), the simulated results indicate multiple resonances with significant dips below -10 dB at approximately 2.5 GHz and 5.5 GHz, suggesting effective impedance matching. The measured S_{11} response follows a similar trend, with a resonance observed at 5.6 GHz, reaching a magnitude of -35 dB. While a slight frequency shift is noted between the simulated and measured results, the overall consistency valid While the fabricated prototype closely aligns with the simulated model, minor discrepancies in resonance frequency and transmission characteristics can be attributed to several key factors.

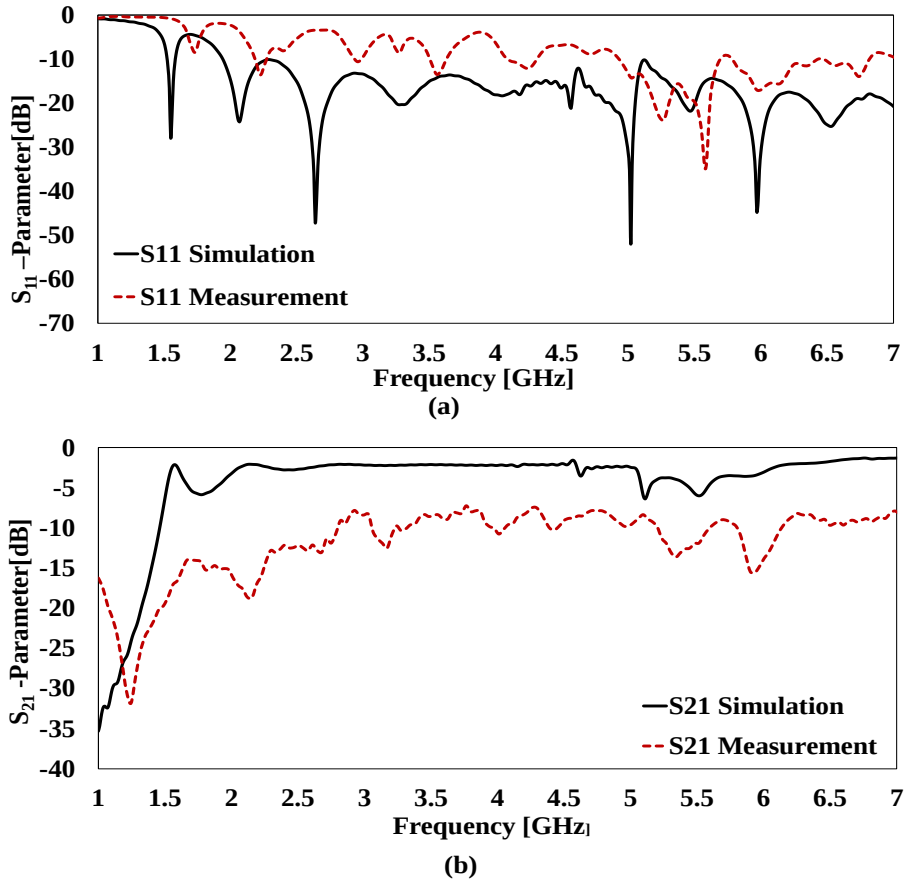

Figure 10. (a) Simulated and fabricated (measured in the experiment) S_{11} for our proposed final SIW antenna. (b) Simulated and fabricated (measured in the experiment) S_{21} for our proposed final SIW antenna.

The first is material variations, as the dielectric properties of PLA can fluctuate due to material composition, infill density, moisture absorption, and temperature changes, which affect impedance matching and radiation efficiency [39]. These effects can be minimized by using high-quality PLA composites, optimizing 3D printing parameters, applying post-processing treatments, and ensuring proper material storage to maintain dielectric consistency [40]. The second factor is fabrication inaccuracies, where minor dimensional errors, surface roughness, and layer inconsistencies introduced during 3D printing can impact resonance frequency and efficiency. These inaccuracies can be reduced by using higher resolution printing settings, refining fabrication precision, and applying conductive coatings to enhance surface conductivity.

Despite these challenges, the fabricated antenna demonstrates strong agreement with simulations, confirming the feasibility of PLA-

based SIW antennas for free-space applications. Further improvements in fabrication precision, material characterization, and VNA calibration will enhance measurement accuracy, ensuring optimized performance for material sensing and wireless communication applications.

5. **Comparison with related research**

This section compares the proposed PLA-based SIW horn antenna with recent advancements in SIW technology, focusing on design type, performance, and practical applications. The comparison considers significant factors such as gain, return loss, material sustainability, and fabrication feasibility. Several SIW-based antenna designs have been explored in the literature, each with unique advantages and trade-offs. Agarwal et al. [41] developed an H-plane SIW Multi-Input Multi-Output (MIMO) horn antenna operating at 3.8 GHz, achieving a gain of 7.92 dB with improved isolation due to closely spaced vias.

However, the design lacked fabrication validation, limiting practical assessment. Nayak et al. [42] introduced a multi-horn SIW antenna at 5.8 GHz, demonstrating good efficiency (86.64%) but at a higher cost due to the Rogers 4232 substrate. Similarly, Nachev et al. [43] integrated a bandpass filter in an SIW horn antenna operating at 6.3 GHz, enhancing frequency selectivity but at the cost of increased complexity and a suboptimal return loss (-20 dB). The emergence of 3D-printed SIW antennas has introduced sustainable and low-cost alternatives. Munir et al. [44] designed a PLA-based slotted SIW antenna for 3–6 GHz applications, demonstrating good agreement between simulation and measurement but suffering from low gain (<0 dB). Another study [45] utilized PLA filament, showcasing lightweight properties but with limited reported gain and frequency range.

In contrast, the proposed PLA-based SIW horn antenna leverages 3D printing for sustainable fabrication while maintaining competitive performance. The design achieves resonant frequencies at 5.02 GHz and 6.0 GHz, with a superior return loss of -52 dB and -44.3 dB, significantly outperforming prior works. The integration of transmitter and receiver functionality enhances compactness and system efficiency. While slight deviations in experimental results were observed (measured resonance at 5.6 GHz, return loss -35 dB), the overall performance confirms the viability of PLA-based antennas for future sensing and communication applications. Table 6 presents a comparative analysis of these SIW antenna designs, highlighting key advancements and limitations. The proposed design stands out due to its optimal balance between cost, sustainability, and high performance, making it a promising candidate for next generation sensing and wireless applications.

6. Conclusion

This study successfully designed, simulated, and fabricated a 3D-printed SIW horn antenna using PLA material, demonstrating its feasibility for wireless and sensing applications. The proposed design optimizes impedance matching and radiation efficiency by integrating dual SIW horn structures on a single PLA substrate, making it suitable for compact, high-frequency applications. Simulation results indicated resonant frequencies at 5.02 GHz and 6.0 GHz, with return losses of -52 dB and -44.3 dB, highlighting excellent performance. Experimental validation using a Vector Network Analyzer (VNA) confirmed a measured resonance at 5.6 GHz with a return loss of -35 dB, indicating substantial agreement despite minor deviations due to fabrication tolerances and PLA's dielectric variability. The use of PLA-based 3D printing presents a sustainable, cost-effective alternative to conventional high-frequency substrates such as Rogers laminates, significantly reducing material costs while maintaining mechanical integrity.

However, fabrication precision and dielectric consistency remain significant challenges in ensuring repeatability across different manufacturing processes. Future work should explore process optimization, improved calibration techniques, and advanced material formulations to enhance dielectric stability and minimize deviations between simulation and

measurement. Additionally, expanding the frequency range and optimizing antenna miniaturization will broaden the applicability of SIW-based antennas in next-generation wireless communication, environmental sensing, and non-destructive material evaluation. Integrating AI-driven data processing for real-time material classification could further enhance the antenna's sensing capabilities, improving accuracy and automation in practical applications. In conclusion, this research validates the potential of 3D-printed SIW antennas as a viable and scalable solution for sensing and communication technologies. With continued advancements in fabrication precision, multi-band SIW structures, and AI-enhanced material characterization, the proposed approach holds significant promise for future sustainable and intelligent wireless applications.

Table 6: Comparative analysis of SIW-based antenna designs

Ref.	Design Type	RF (GHz)	Gain (dB)	RL (dB)	Significant Features	Advantages	Limitations
[41]	MIMO with H-plane SIW antennas	3.8	7.92	-35	Closely spaced vias to reduce coupling	High gain, reduced mutual coupling	No fabrication validation
[42]	Multi-horn SIW antennas	5.8	5.6	-20	Multi-horn on a single substrate	Compact multi-horn design for directional applications	Moderate return loss
[43]	SIW H-plane horn antenna	6.3	5.15	-38	Integrated bandpass filter	Improved frequency selectivity with filter integration	Increased fabrication complexity
[8]	Compact Wideband SIW Horn Antenna	17.4-24	8	>-10	more compact in size	Wide bandwidth and novel feeding structure.	dielectric loss and the fabrication tolerance.
[44]	PLA-based slotted SIW antenna	3.3, 5.24	<0 dB	-30, -25	3D-printed slotted SIW design	Low-cost, sustainable 3D-printed material	Very low gain, limiting wireless applications
[45]	SIW using PLA filament	1.92–4.22	NA	-35	Lightweight, low-cost PLA design	Cost-effective with good mechanical properties	Limited frequency range and lack of detailed gain data
This work	PLA-based integrated SIW horn antennas	5.02, 6.0	5.43	-52, -44.3	Integrated transmitter/receiver, 3D-printed PLA material	Best return loss, sustainable material, cost-effective	Slight frequency shift in experimental validation

RL=Return Loss, RF=Resonance frequence

Acknowledgment

The authors thank the Universiti Malaysia Pahang Al-Sultan Abdullah for laboratory facilities and financial support under Internal Research Grant RDU220382.

References

[1] G. M. Rocco, M. Bozzi, S. Marconi, G. Alaimo, F. Auricchio and D. Schreurs, "3D-printed microfluidic sensor in substrate integrated waveguide technology," In *2018 IEEE MTT-S International Microwave Workshop Series on Advanced Materials and Processes for RF and THz Applications (IMWS-AMP)*, pp. 1-3. IEEE, 2018. DOI: 10.1109/IMWS-AMP.2018.8457168.

[2] N. Hasan, N. S. M. Hussain, A.A.M. Faudzi, S. M. Shaharum, N.A.T. Yusof, N. H. Noordin, N.A.A. Mohtadzar and M. S. A. Karim, "Cured epoxy resin dielectric characterization based on accurate waveguide technique," In *AIP Conference Proceedings*, vol. 2129, no. 1. AIP Publishing, 2019. DOI: 10.1063/1.5118088.

[3] N. S. Khair, N. A. T. Yusof, Yasmin A. Wahab, B. S. Bari, N. I. Ayob and M. Zolkapli, "Substrate-integrated waveguide (SIW) microwave sensor theory and model in characterising dielectric material: A review," *Sensors International* (2023): 100244. DOI: 10.1016/j.sintl.2023.100244.

[4] A. H. Allah, G. A. Eyebe, and F. Domingue, "Fully 3D-printed microfluidic sensor using substrate integrated waveguide technology for liquid permittivity characterization," *IEEE Sensors Journal* 22, no. 11, 2022, 10541-10550. DOI: 10.1109/JSEN.2022.3170507.

[5] N. A. T. Yusof, N. Zainol, N. H. Aziz, and M. S. A. Karim, "Effect of fiber morphology and elemental composition of Ananas comosus leaf on cellulose content and permittivity," *Current Applied Science and Technology*, 2023,10-55003. DOI: 10.55003/cast.2023.06.23.002.

[6] S. Huang, K. Y. Chan, and Rodica Ramer, "Dielectric-loaded SIW H-plane horn antenna with gradient air slots." *IEEE Antennas and Wireless Propagation Letters* 20, no. 1, 2020, 43-47. DOI: 10.1109/LAWP.2020.3039265.

[7] S.M Shaharum., N.H. Hashim, N.A.T@ Yusof, A. Karim, and A.A. M Faudzi, "Automatic detection of diabetic retinopathy retinal images using artificial neural network". In *Proceedings of the 10th National Technical Seminar on Underwater System Technology 2018, NUSYS'18*, pp. 495-503, Springer Singapore. DOI:10.1007/978-981-13-3708-6_43

[8] Y. Cai, Z. Qian, W. Cao, Y. Zhang, J. Jin, L. Yang, and N. Jing, "Compact wideband SIW horn antenna fed by elevated-CPW structure." *IEEE Transactions on Antennas and Propagation* 63, no. 10, 2015, 4551-4557. DOI: 10.1109/TAP.2015.2456936

[9] D. Sun, J. Xu, and S. Jiang, "SIW horn antenna built on thin substrate with improved impedance matching." *Electronics Letters* 51, no. 16, 2015, 1233-1235. DOI: 10.1049/el.2015.1396.

[10] N.S. Khair, N. A. T. Yusof, M. H. M. Ariff, Y. A. Wahab, and B. S. Bari. "Recent advances and open challenges in RFID antenna applications." *Enabling Industry 4.0 through Advances in Mechatronics: Selected Articles from iM3F 2021, Malaysia* (2022): 507-517. DOI: 10.1007/978-981-19-2095-0_43.

[11] K. R. Brinker, and R. Zoughi, "A review of chipless RFID measurement methods, response detection approaches, and decoding techniques," *IEEE Open Journal of Instrumentation and Measurement* 1, 2022, 1-31. DOI: 10.1109/OJIM.2022.3196746.

[12] R. Colella, F. P. Chietera, F. Montagna, A. Greco and L. Catarinucci, "Customizing 3D-Printing for Electromagnetics to Design Enhanced RFID Antennas," in *IEEE Journal of Radio Frequency Identification*, vol. 4, no. 4, pp. 452-460, Dec. 2020. DOI: 10.1109/JRFID.2020.3001043.

[13] M. Z. E. Syefrizal, N. A. T. Yusof, M. S. A. Karim, N. Hasan and N. F. Zakaria, "Design of Vivaldi antenna for non-destructive measurement applications.", *Engineering Technology International Conference (ETIC 2022)*, Online Conference, Kuantan, Malaysia, 2022, pp. 356-363. DOI: 10.1049/icp.2022.2644.

[14] N.A.T@ Yusof, S. M. Shaharum, A. A. M. Faudzi, S. Khatun, M. S. A. Karim, and S. F. Hazali. "Design of Ultra-Wideband (UWB) Horn Antenna for Non-destructive Fruit Quality Monitoring." In *Proceedings of the 10th National Technical Seminar on Underwater System Technology 2018: NUSYS'18*, pp. 515-521. Springer Singapore, 2019. DOI: 10.1007/978-981-13-3708-6_45.

[15] S. S. Carvalho, J. R. V. Reis, A. Mateus and R. F. S. Caldeirinha, "Exploring Design Approaches for 3D Printed Antennas," in *IEEE Access*, vol. 12, pp. 10718-10735, 2024. DOI: 10.1109/ACCESS.2024.3354372.

[16] S.Huang, K. Y. Chan, Y. Wang, and R. Ramer. "High gain SIW H-plane horn antenna with 3D printed parasitic E-plane horn." *Electronics* 10, no. 19, 2021, 2391. DOI: 10.3390/electronics10192391.

[17] B. S. Bari, S. Khatun, K. H. Ghazali, M. Islam, M. Rashid, M, Rahman, and N. A. Talip, "Performance comparison of early breast cancer detection precision using AI and Ultra-Wideband (UWB) bio-antennas." In *Cyber Security and Computer Science: Second EAI International Conference, ICONCS 2020, Dhaka, Bangladesh, February 15-16, 2020, Proceedings 2*, pp. 354-365. Springer International Publishing, 2020. DOI: 10.1007/978-3-030-52856-0_28.

[18] M. M. Alam, A. A. F. Faudzi, S. M. Shaharum, Y. A. Wahab, M. H. A. A. Malek, M. S. A. Karim and N. A. T. Yusof., "Design and analysis of triple-band SIW antenna for K-Band and Ka-Band applications", *International Exchange and Innovation Conference on Engineering & Sciences*, Japan, 2024. DOI: 10.5109/7323346.

[19] J. Olivová., M. Popela., M. Richterová and E. Štefl., 2022. "Use of 3D printing for horn antenna manufacturing", *Electronics*, *11*(10), p.1539. DOI: 10.3390/electronics11101539.

[20] H. Amer and M. A. K. Abdulsattar, "Design of substrate integrated waveguide (SIW)

antenna," *Communications on Applied Electronics* 7, no. 17, 2018, 14-20. DOI: 10.5120/cae2018652774.

[21] Y. Alnaiemy and L. Nagy, "Improved antenna gain and efficiency using novel EBG layer," In *2020 IEEE 15th International Conference of System of Systems Engineering (SoSE)*, pp. 271-276. IEEE, 2020. DOI: 10.1109/SoSE50414.2020.9130494.

[22] K. Anusha, K. Karthika, D. Mohanageetha, A. Monika, S. V. N S. Kumar, and B. Lavanya. "Gain enhancement of circular patch antenna using SRR array," In *2021 International Conference on Advancements in Electrical, Electronics, Communication, Computing and Automation (ICAECA)*, pp. 1-5. IEEE, 2021. DOI: 10.1109/ICAECA52838.2021.9675499.

[23] H. Jin and X. Jing, "A Novel Humidity Sensor Based on Slow-Wave Substrate Integrated Waveguide," In *2024 IEEE International Symposium on Antennas and Propagation and INC/USNC-URSI Radio Science Meeting (AP-S/INC-USNC-URSI)*, pp. 27-28. IEEE, 2024. DOI: 10.1109/AP-S/INC-USNC-URSI52054.2024.10686746

[24] C. M. Chen, L. Chen, Y. Yao, and Y. Peng. "Flexible SIW humidity sensors based on nanodiamond sensing films," International Journal of Microwave and Wireless Technologies 15, no. 9, 2023, 1475-1482.DOI: 10.1017/S1759078723000363

[25] M. Amiri, M. Abolhasan, N. Shariati, and J. Lipman, "Soil moisture remote sensing using SIW cavity based metamaterial perfect absorber," *Scientific Reports*, 11, no. 1 (2021): 7153.DOI: 10.1038/s41598-021-86194-2.

[26] M.S.A.Karim, N. Zainol, N.I.A.A.H. As'ari, N.A.T. Yusof and N.H. Aziz, 2022, "Effect of processing parameters on cellulose content extracted from pineapple leaf." *Biocatalysis and Agricultural Biotechnology*, *42*, p.102339. DOI: 10.1016/j.bcab.2022.102339.

[27] L. Kumar, V. Nath and B.V.R. Reddy, 2023, "A wideband substrate integrated waveguide (SIW) antenna using shorted vias for 5G communications" *AEU-International Journal of Electronics and Communications*, *171*, p.154879.DOI: 10.1016/j.aeue.2023.154879.

[28] Galka, A. Georgievich, A. V. Kostrov, S. E. Priver, A. V. Strikovskiy, V. V. Parshin, E. A. Serov, A. S. Nikolenko, S. V. Korobkov, and M. E. Gushchin, "Microwave Cavity Sensor for Measurements of Air Humidity under Reduced Pressure", *Sensors* 23, no. 3, 2023, 1498. DOI: 10.3390/s23031498.

[29] J. Chocarro, J. M. P. Escudero, J. Teniente, J. C. I. Galarregui and I. Ederra, "A metasurface-enhanced substrate-integrated waveguide Antenna," *IEEE Access*, 2024. DOI: 10.1109/ACCESS.2024.3394698.

[30] V.Kumari, W. Bhowmik, and S. Srivastava. "Design of high-gain SIW and HMSIW H-plane horn antenna using metamaterial." *International Journal of Microwave and Wireless Technologies* 7, no. 6 (2015): 713-720. DOI: 10.1017/S1759078714000920.

[31] M. Farashahi, E. Z. Jahromi, and R. Basiri. "A compact semi-open wideband SIW horn antenna for K/Ku band applications." *AEU-International Journal of Electronics and Communications* 92 (2018): 15-20. DOI: 10.1016/j.aeue.2018.05.012.

[32] Z. Gholipour, and J. A. Shokouh. "Substrate integrated waveguide corrugated horn antenna." *Wireless Personal Communications* 109, 2019,1605-1614. DOI: 10.1007/s11277-019-06640-3.

[33] R. Colella, F. P. Chietera, and L. Catarinucci. "Analysis of FDM and DLP 3D-printing technologies to prototype electromagnetic devices for RFID applications." *Sensors* 21, no. 3 (2021): 897. DOI: 10.3390/s21030897.

[34] E. Huber, M. Mirzaee, J. Bjorgaard, M. Hoyack, S. Noghanian, and I. Chang. "Dielectric property measurement of PLA." In *2016 IEEE International Conference on Electro Information Technology (EIT)*, pp. 0788-0792. IEEE, 2016. DOI: 10.1109/EIT.2016.7535340.

[35] T.M. Joseph, A. Kallingal, A. M. Suresh, D. K. Mahapatra, M. S. Hasanin, J. Haponiuk, and S. Thomas. "3D printing of polylactic acid: recent advances and opportunities." *The International Journal of Advanced Manufacturing Technology* 125, no. 3 (2023): 1015-1035. DOI: 10.1007/s00170-022-10795-y.

[36] X. Wang, L. Huang., Y. Li., Y. Wang, Lu, X., Wei, Z., Mo, Q., Zhang, S., Sheng, Y., Huang, C. and Zhao, H., 2024, "Research progress in polylactic acid processing for 3D printing", *Journal of Manufacturing Processes*, *112*, pp.161-178. DOI: 10.1016/j.jmapro.2024.01.03.

[37] G. Liu, C. Wang, Z. Jia, K. Wang, W. Ma and Z. Li, "A Rapid Design and Fabrication Method for a Capacitive Accelerometer Based on Machine Learning and 3D Printing Techniques", in *IEEE Sensors Journal*, vol. 21, no. 16, pp. 17695-17702, 15 Aug.15, 2021. DOI: 10.1109/JSEN.2021.3085743.

[38] A.K.Kesarwani, M. Yadav, D. Singh, and G. D. Gautam. "A review on the recent applications of particle swarm optimization & genetic algorithm during antenna design." *Materials Today: Proceedings* 56 (2022): 3823-3825. DOI: 10.1016/j.matpr.2022.02.200

[39] R.R. Holkar., G. G. Umarji, M. D. Shinde, and S. B. Rane. "3D printing of microwave materials, components and their applications–A review." *Journal of Manufacturing Processes* 137 (2025): 280-305. DOI: 10.1016/j.jmapro.2025.02.006.

[40] D. Srinivasan, M. Meignanamoorthy, M. Ravichandran, V. Mohanavel, S. V. Alagarsamy, C. Chanakyan, S. Sakthivelu, Alagar Karthick, T. Ram Prabhu, and S. Rajkumar, "3D printing manufacturing techniques, materials, and applications: an overview." *Advances in materials science and engineering* 2021, no. 1 (2021): 5756563. DOI: 10.1155/2021/5756563.

[41] T. Agrawal and S. Srivastava, "Two element MIMO antenna using Substrate Integrated Waveguide (SIW) horn," In *2016 International Conference on Signal Processing and Communication (ICSC)*, pp. 508-511. IEEE, 2016. DOI: 10.1109/ICSPCom.2016.7980633.

[42] I. Nachev and I. Iliev. "A simplified methodology for h-plane siw horn antenna design," In *2023 58th International Scientific Conference on Information, Communication and Energy Systems and Technologies (ICEST)*, pp. 245-248. IEEE, 2023. DOI: 10.1109/ICEST58410.2023.10187258.

[43] A. K. Nayak, V. S. Yadav and A. Patnaik, "An H-plane multi-horn antenna using substrate integrated waveguide technique," In *2021 National Conference on Communications (NCC)*, pp. 1-4. IEEE, 2021. DOI: 10.1109/NCC52529.2021.9530167.

[44] A. Munir, B. Syihabuddin, M. F. Maulana and R. Aulia, "Characterization of a 3D-printed PLA-based slotted SIW antenna," In *2023 Workshop on Microwave Theory and Technology in Wireless Communications (MTTW)*, pp. 128-131. IEEE, 2023. DOI: 10.1109/MTTW59774.2023.10320082.

[45] Y. Kim and S. Lim, "Low loss substrate-integrated waveguide using 3D-printed non-uniform honeycomb-shaped material." *IEEE Access* 8, 2020, 191090-191099. DOI: 10.1109/ACCESS.2020.3032132.